http://dx.doi.org/10.21577/0100-4042.20170950 *Quim. Nova,* Vol. 46, No. 1, 20-28, 2023

Artigo

REDUCING NON-SPECIFIC ADSORPTION OF PROTEINS VIA THE HPG MODIFICATION ON THE SURFACE OF MAGNETIC NANOPARTICLES

Meng Zhou[a], Chunyu Sun[a] and Hong Zhao[a,*]
[a]School of Chemistry and Chemical Engineering, Southeast University, Nanjing 211189, China

Recebido em 17/02/2022; aceito em 31/08/2022; publicado na web em 26/09/2022

Reducing non-specific adsorption of proteins on the surface of magnetic nanoparticles (MNPs) is becoming increasingly important. In this paper, we proposed a novel surface modification procedure by grafting hyperbranched polyglycerol (HPG) onto the surface of MNPs (Fe_3O_4@SiO_2@MAA), in which lots of hydroxyl groups from HPG not only provide the hydrates sheath to prevent non-specific adsorption of proteins, but also react with succinic anhydride to generate carboxyl groups that serve as active sites to specifically bind proteins. The protein adsorption experiments showed that the non-specific adsorption (0.07 μg mg^{-1}) was reduced to 4.58% of that before modification. It also showed that the antigen binding capacity was 9.7 times higher than the original when detecting cardiac troponin I (cTnI) in human plasma samples, which indicated that the final synthesized MNPs had great application prospects in bio-separation and bioanalysis.

Keywords: anti-protein adsorption; hyperbranched polyglycerol; magnetic nanoparticles; phycoerythrin; cardiac troponin I.

INTRODUCTION

In recent years, magnetic nanoparticles have been widely used in protein purification,[1-8] drug delivery,[9-11] bacterial detection and other fields[12-16] due to their strong magnetic properties, large specific surface area, controllable size and easy separation.[17-20] In 1993, Ugelstad *et al.* synthesized series of magnetic nanoparticles (MNPs) with the commercial brand "Dynabeads" by swelling and absorbing magnetic particles of polymer microspheres for the first time.[21] This method opened up a milestone of monodisperse magnetic polymer microspheres, which has been successfully applied in many fields such as microbiology, molecular biology and immunology. At present, the big advances have been made on the synthesis of magnetic composite microspheres. However, there are still some problems to be solved in the practical application, such as how to decrease the non-specific adsorption of proteins in the conjugation of antigen or antibody molecules on their surface. The non-specific adsorption of proteins will lead to many adverse effects. For example, although immuno-magnetic technology for *in vitro* detection of circulating tumor cells has shown promising potential for clinical applications, non-specific adhesion of biomolecules and non-cancerous cells in complex biological samples to the surface of magnetic materials, can reduce the sensitivity and specificity of cell detection.[22] Therefore, it is of great significance to reduce the non-specific adsorption of proteins on the surface of materials.

There are many kinds of anti-protein adsorption materials and various classification methods. In this paper, we classify anti-protein adsorbents into two classes according to their molecular structure: non-amphoteric hydrophilic polymers[23-28] and zwitterionic materials with both positive and negative charge centers,[29-34] the first is represented by polyethylene glycol (PEG) and its derivatives. In 2010, Chen *et al.* investigated the influence of molecular weights and chain densities of PEGxk on the non-specific binding of PEGylated MNPs to human serum protein, the optimal molecular weight and chain density were determined.[34] In 2021, Kim *et al.* synthesized silica-shell-coated magnetic nanoparticles and modified them with zwitterionic and primary amine ligands. The results showed that nonspecific adsorption with biomolecules onto surface were significantly suppressed.[33] Polyethylene glycol (PEG) and its derivatives are generally believed to have the ability to resist non-specific adsorption of proteins through the formation of a physical and energy barrier by very tightly bonded water molecules on the surface of materials. In 2013, Slovakia *et al.* synthesized the MNPs with PEG in an almost spherical shape.[23] *In vitro* toxicity of the magnetic fluids using cells of skin cancer of mice B16 was tested and confirmed the good biocompatibility of the prepared MNPs. In 2014, Bilkova *et al.* confirmed the PEGylated MNPs displayed a pronounced reduction of protein adsorption and cellular uptake respect to bare MNPs.[24] However, due to the thermal instability and rapid autooxidation of PEG, it is necessary to develop the alternative antifouling materials.

In recent years, hyperbranched polyglycerol (HPG) was widely used in biomedicine, coatings, separation membranes and other fields due to its good biocompatibility and anti-pollution properties.[35-38] HPG can be regarded as a derivative of PEG, and it is also a hydrophilic polymer material with a highly branched structure. It has high solubility in water because of its molecular end with a large number of hydroxyl groups. In 1996, Irvine *et al.* predicted theoretically that a given branched polymer will be more efficient in preventing nonspecific protein adsorption and specific cell adhesion than its linear analogue.[39] Previous studies mainly generated HPG directly on the surface of MNPs;[35] however, those magnetic particles had small particle size, low saturation magnetization value and long magnetic separation time.

Based on the above understanding, we creatively designed an organic synthesis route, first synthesized HPG, then grafted HPG and active carboxyl groups on the surface of Fe_3O_4@SiO_2@MAA, and finally obtained MNPs with a particle size of 845.04 nm.The magnetic separation process can be completed in 20 seconds, and the magnetic nanoparticles had good anti-protein adsorption performance and stability in complex biological environment. It was also confirmed that the detection of cardiac troponin I (cTnI) in human plasma samples was more efficient when it was made into sandwich chemiluminescence immunomagnetic than before grafting HPG.[40-42]

*e-mail: zhaohong@seu.edu.cn

EXPERIMENTAL

Materials

Amberlite® IR-120, Succinic anhydride (SA), *N,N*-methylene bisacrylamide (MBA) and 2,2-azodiisobutyronitrile (AIBN) were purchased from Aladdin (Shanghai, China). Potassium methoxide, 4-dimethylaminopyridine (DMAP), 4,4'-Azobis (4-cyanovaleric acid) (MDI), glycerinum, 1,1,1-Tris(hydroxymethyl)propane (TMP), glycidyl (2,3-epoxy-1-propanol) and α-methacrylic acid (MAA) were commercially available from Macklin (Shanghai, China). Phycoerythrin freeze-dried powder was purchased from Seebio Biotech (Shanghai) Co., Ltd. Ferric chloride hexahydrate ($FeCl_3{\cdot}6H_2O$), ethanol, ammonia, *N,N*-dimethylformamide (DMF), acetonitrile, tetraethyl orthosilicate, methanol, acetone were obtained from Sinopharm Chemical Reagent Co., Ltd. 1-Ethyl-3-(3-dimethylaminopropyl) carbodiimide hydrochloride (EDC), *N*-hydroxy succinimide (NHS), 2-morpholinoethanesulfonic acid (MES) and phosphate buffer saline (PBS) were purchased from Shanghai Yuanye Co., Ltd (China). The chemicals used in this research were analytical grade and used without further treatment unless otherwise mentioned. All aqueous solutions were prepared using distilled water.

Synthesis of HPG

HPG was synthesized via anionic ring-opening polymerization according to the method of the literature.[35] First, 0.278 g of 1,1,1-Tris(hydroxymethyl)propane was added in the three-neck flask, heated to 75 °C in a nitrogen atmosphere, then added 0.0648 g of methoxide, and the reaction temperature was raised to 95 °C, and 20 mL of glycidyl (2,3-epoxy-1-propanol) was slowly added through the constant pressure dropping funnel. After the drop addition of 12 h, the final product was dissolved in 40 mL of methanol and then passed through the cation exchange resin. At this time, the resulting solution was transferred to 10 times the volume of acetone for deposition to obtain the crude product, and then the crude product was dissolved with methanol, and finally the methanol was removed by the rotary evaporator. The pale yellow transparent liquid was obtained, and the methanol was dried in a vacuum drying oven and sealed for refrigeration (Figure 1).

Synthesis of Fe_3O_4@SiO_2@MAA-HPG-COOH

The following synthesis route was designed to graft HPG and carboxyl groups to Fe_3O_4@SiO_2@ MAA. Fe_3O_4@SiO_2@MAA was synthesized by the method reported in literature.[43] Firstly, 0.1 g of Fe_3O_4@SiO_2@MAA was uniformly dispersed in 20 mL of DMF, and 0.5 g of MDI was added, ultrasound was performed for 10 minutes to evenly distribute them, and the reaction was performed at 80 °C for 24 h. Then magnetic separation was performed and re-dispersed in 20 mL of DMF, and 0.1 g of HPG was added, and the reaction was performed at 80 °C for 12 h. Finally, magnetic separation was performed again, re-dispersed in 20 mL of DMF, added 0.1 g of SA and 0.1 g of DMAP, and reacted at 80 °C for 12 h. When the reaction was complete, the final product was separated with magnets, washed with ethanol and distilled water, and dispersed in distilled water for later use (Figures 2 and 3).

Protein adsorption experiments

It is important to evaluate the amount of non-specific adsorption and specific binding of MNPs to proteins. To evaluate the non-specific adsorption, a certain amount of MNPs was added to the phycoerythrin solution with a certain concentration, and mixed evenly on the shaker at 37 °C. After 3 h of reaction, the supernatant was separated with magnets, and the fluorescence intensity of the supernatant before and after the reaction with the MNPs was measured. The non-specific adsorption amount was calculated according to the standard curve. In the evaluation of specific binding affinity, the carboxyl MNPs were activated by EDC and NHS in MES solution, and then reacted with phycoerythrin solution. The amount of specific binding was calculated

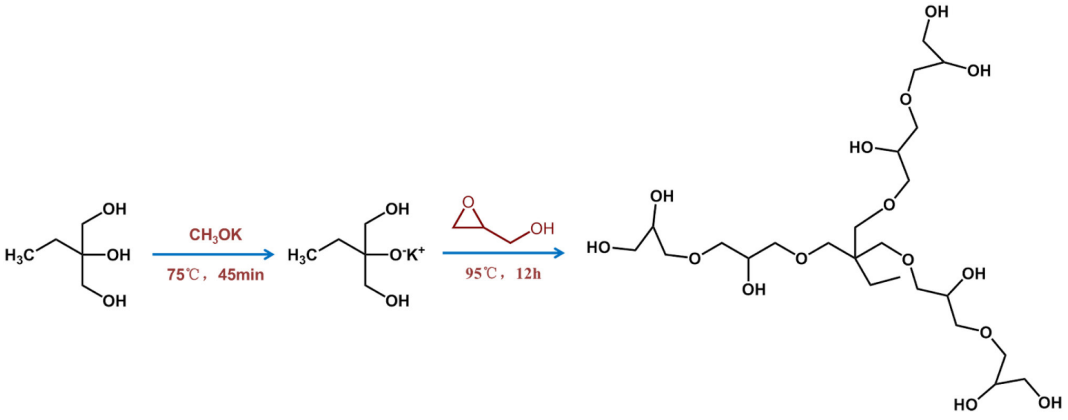

Figure 1. *Preparation process of HPG*

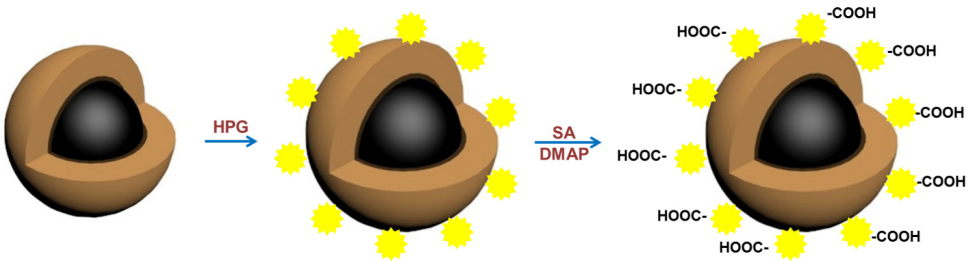

Figure 2. *Diagram of synthesis of Fe_3O_4@SiO_2@MAA-HPG-COOH*

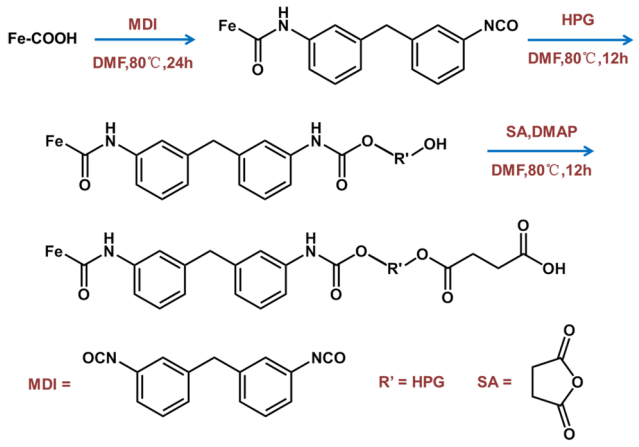

Figure 3. *Preparation process of Fe_3O_4@SiO_2@MAA-HPG-COOH*

according to the change of fluorescence intensity of supernatant before and after incubation with phycoerythrin.[44,45]

Chemiluminescence immunoassay experiments

In order to evaluate the practical application of MNPs, we developed a sandwich-type chemiluminescence immunoassay method for the quantitative detection of cTnI in plasma by acridinium ester-labeled anti-cTnI (Figure 4). Firstly, streptavidin was labeled to the MNPs by the active ester method. Then, the biotin-labeled anti-cTnI was bound to the MNPs by the strong interaction between streptavidin and biotin. The MNPs obtained in this step were added to the plasma to bind specifically to the cTnI. Finally, the MNPs attached to the antibody- antigen complex react with the acridinium ester-labeled anti-cTnI to detect the cTnI in the sample.[40-42]

Material characterization

The morphology and size distribution of nanoparticles were characterized by scanning electron microscopy (SEM, FEI Inspect F50) and transmission electron microscopy (TEM, FEI G20). The thermal properties of these nanoparticles were investigated by thermo gravimetry (TG). Dynamic light scattering (DLS) was used to analyze particle size and monodispersity. The saturation magnetization of nanoparticles was evaluated by a vibrating sample magnetometer (VSM, LakeShore7404). X-ray diffraction (XRD) was used to evaluate the crystal structure of ferric oxide in nanoparticles. The molecular formula of HPG was determined by hydrogen nuclear magnetic resonance spectroscopy (NMR). Matrix-assisted laser desorption ionization time of flight mass spectrometry (MALDI-TOF-MS) was used to determine the relative molecular mass of HPG. Fourier transform infrared spectroscopy (Nicolet 5700 FTIR) was used to prove that HPG contains multiple hydroxyl groups and the chemical structure of the products at each step in the synthesis process. Particle size and the surface charge were analyzed by dynamic light scattering (DLS, Brookhaven, US) with a zeta electrode. The photoluminescence (PL) spectra were used to characterize the fluorescence properties of phycoerythrin solution.

RESULTS AND DISCUSSION

Characterization of HPG

HPG was prepared by one-step anionic ring-opening polymerization using 1,1,1-Tris(hydroxymethyl)propane as initiator and glycidyl (2,3-epoxy-1-propanol) as monomer.[35] HPG was characterized by ^{1}H NMR, MALDI-TOF-MS, FTIR and TG. As shown in Figure 5a, the average relative molecular mass of HPG is about 500-600 according to MALDI-TOF-MS. The FTIR (Figure 5b) showed that HPG has a large absorbance at the position of characteristic stretching absorption peak of hydroxyl group at 3650-3200 cm^{-1} and 1200-1150 cm^{-1}, which proved that HPG might be a multi-hydroxyl structure. Thermogravimetric analysis (Figure 5c) showed that HPG began to decompose at 375 °C, and the decomposition temperature was high, indicating that HPG had good thermal stability.

The branched structure of HPG can be indicated by ^{1}H NMR in D_2O (Figure 5d).[35] ^{1}H NMR (600 MHz, D_2O) δ ppm 4.99–4.64 (m, 30H), 4.08–3.80 (m, 28H), 3.80–3.32 (m, 105H), 1.55–1.32 (m, 1H), 1.24–0.63 (m, 1H).HPG displayed a predominant signal in 3.32–3.80 ppm due to C<u>H</u>-OH and CH_2-O<u>H</u>, the peak arisen in 4.64–4.99 ppm, attributable to O–C<u>H</u>$_2$-C and CH-O<u>H</u>, two small but visible peaks were present at 1.32-1.55 and 0.63-1.24 ppm caused by -C<u>H</u>$_2$-C<u>H</u>$_3$. Combined with the chemical reaction equation, the molecular structure formula of HPG can be predicted, the number and the area of peaks in different chemical environments in Figure 5d can be matched with the ^{1}H NMR spectrum of M=578.31 predicted by ChemDraw software. The product was not purified, so there was a small amount of HPG with a relative molecular weight greater than 578.31 in the product. Therefore, the area of the peak cannot correspond well with the number of hydrogen in different chemical environments in the molecular formula M=578.31.

The FTIR of the prepared HPG contained the characteristic absorption peak of hydroxyl group, and the ^{1}H NMR was consistent with the reference literature, which indicates that HPG has been

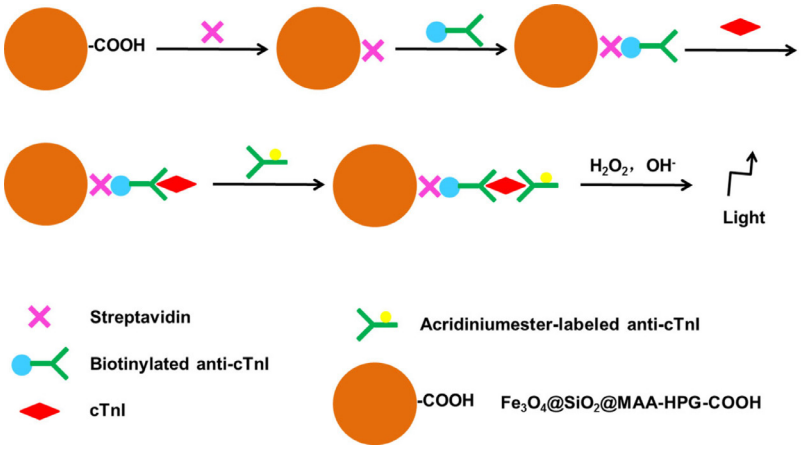

Figure 4. *Preparation process of sandwich-type chemiluminescence immunoassay method*

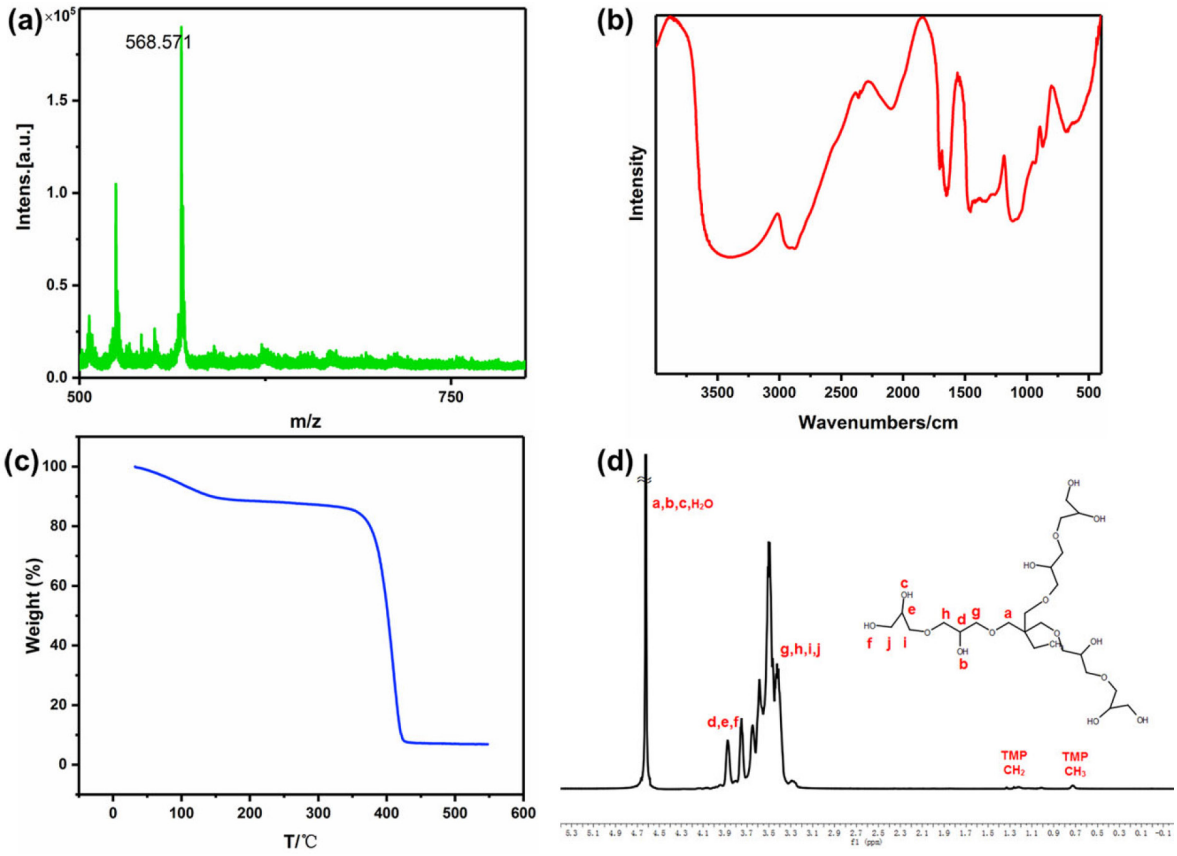

Figure 5. *HPG was characterized by (a) MALDI-TOF-MS, (b) FTIR and (c) TG and (d) ^1H NMR*

successfully prepared. The compound contained multiple hydroxyl groups, which were easy to react with other compounds and had good water solubility. It can be predicted that if HPG was modified on the surface of MNPs, it will greatly improve the stability in water.

Characterization of Fe_3O_4@SiO_2@MAA-HPG-COOH

The carboxylic magnetic particles Fe_3O_4@SiO_2@MAA were prepared by precipitation polymerization, and reacted with HPG to achieve the purpose of modifying a lot of hydroxyl groups on the surface of Fe_3O_4@SiO_2@MAA. Then the hydroxyl groups reacted with SA to obtain magnetic nanoparticles with both hydroxyl and carboxyl groups on the surface. SEM, TEM, TG, XRD, VSM and FTIR were used to characterize the products at different reaction stages.

Morphology and size distribution

In order to characterize the morphology and size distribution of magnetic nanoparticles, SEM and TEM were used. Figure 6a showed the surface morphology of Fe_3O_4 nanoparticles coated with a layer of MAA. It can be seen that the surface was very smooth. Figure 6b showed that the surface of the final product become significantly rougher compared with that of the previous step, indicating that new substances grow on it, which was considered to be a large amount of MDI and HPG deposited on the surface of Fe_3O_4@SiO_2@MAA. HPG can be regarded as a derivative of PEG and had good anti-protein nonspecific adsorption ability. Figure 7b) showed TEM images of products at different stages of reaction, corresponding to SEM images one by one. It can be seen that the polymer layer coated on the surface was very thick. Multiple particles in the same picture were measured

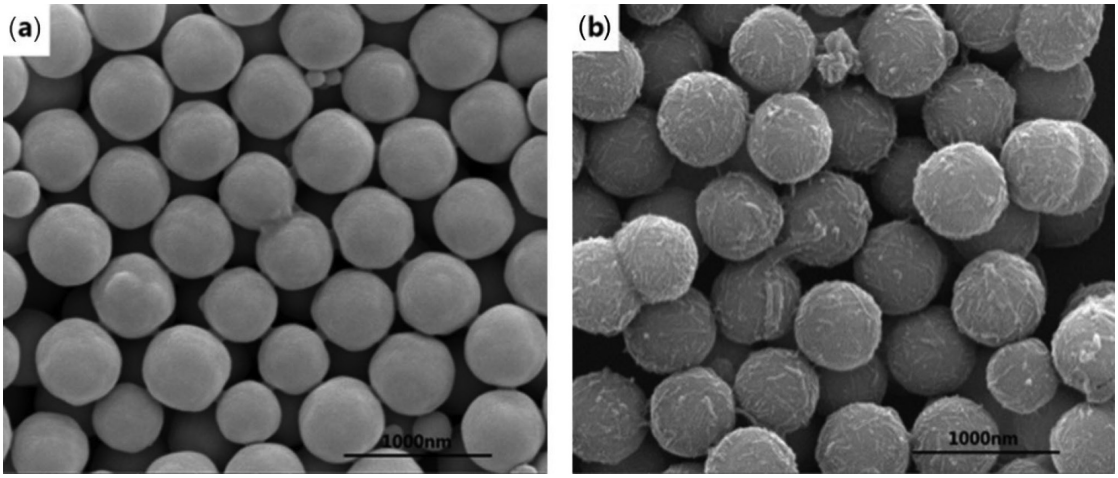

Figure 6. *SEM images of (a) Fe_3O_4@SiO_2@MAA and (b) Fe_3O_4@SiO_2@MAA-HPG-COOH*

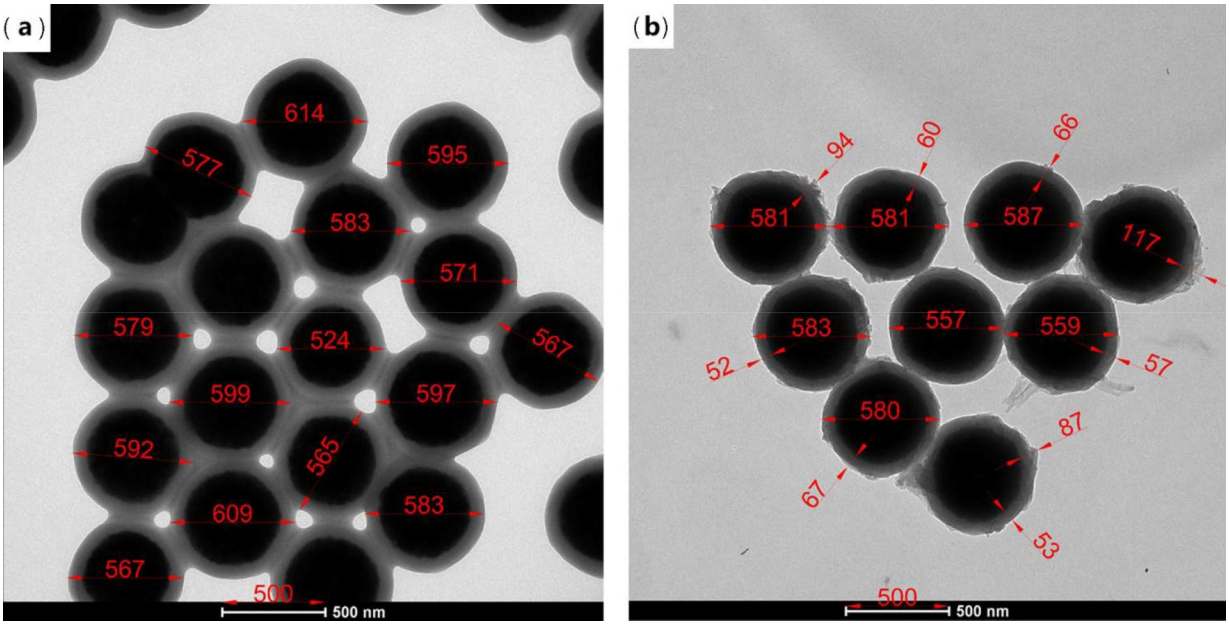

Figure 7. *TEM images of (a) Fe_3O_4@SiO_2@MAA and (b) Fe_3O_4@SiO_2@MAA-HPG-COOH*

by AutoCAD software, and the shell thickness of the modified product was about 90 nm, and the diameter of MNPs was about 600 nm.[46]

XRD and VSM characterization

XRD and VSM characterization were used to characterize the products at different stages of the whole reaction process to ensure that the crystal structure of ferric oxide was not destroyed and the superparamagnetism of MNPs was not changed. Figure 8a showed the XRD patterns of Fe_3O_4, Fe_3O_4@SiO_2@MAA and Fe_3O_4@SiO_2@MAA-HPG-COOH respectively. It can be seen that compared with the standard card of Fe_3O_4, the peaks at 2θ = 18.38, 30.08, 35.45, 42.88, 56.75 and 62.10 correspond to the crystal planes of Fe_3O_4 (111), (220), (311), (400), (333) and (440), respectively, indicating that the Fe_3O_4 crystal type was not destroyed during the reaction process.

Figure 8b showed the magnetization curves of Fe_3O_4, Fe_3O_4@SiO_2@MAA, and Fe_3O_4@SiO_2@MAA-HPG-COOH. Magnetic test results showed that the saturation magnetization value of Fe_3O_4 reached 89.60 emu g^{-1}, the saturation magnetization value of Fe_3O_4@SiO_2@MAA was 50.05 emu g^{-1}, and the saturation magnetization value of the final product Fe_3O_4@SiO_2@MAA-HPG-COOH was 44.75 emu g^{-1}. Figure 8b showed that none of the three has magnetic hysteresis, they had strong superparamagnetism.[43] Therefore, the decrease of saturation magnetization is due to the influence of polymer coating on the MNPs.[47]

FTIR spectra were employed to examine the surface groups of the nanoparticles obtained at each stage (Figure 9). It can be seen that the characteristic absorption peaks of Fe-O bond existed in all the five spectral lines at 607 cm^{-1}, which was consistent with the introduced Fe_3O_4 magnetic core. The characteristic absorption peak at 1700 cm^{-1} (Figure 9b) was attributed to the carboxyl group in the shell material MAA, indicating that the organic polymer MAA had successfully coated the surface of Fe_3O_4 nanoparticles. MDI can form dimers or trimers during the reaction process, so Fe_3O_4@SiO_2@MAA has an amino group after MDI modified, which was confirmed by the absorption peaks of N-H bonds at 817 cm^{-1} and 1512 cm^{-1} (Figure 9c). The characteristic absorption peak of O-H bond appeared at 3309 cm^{-1} (Figure 9d), indicating that HPG was successfully grafted onto MNPs. Finally, the terminal -OH of Fe_3O_4@SiO_2@MAA-HPG was converted to -COOH by reacting with succinic anhydride, and the characteristic absorption peak

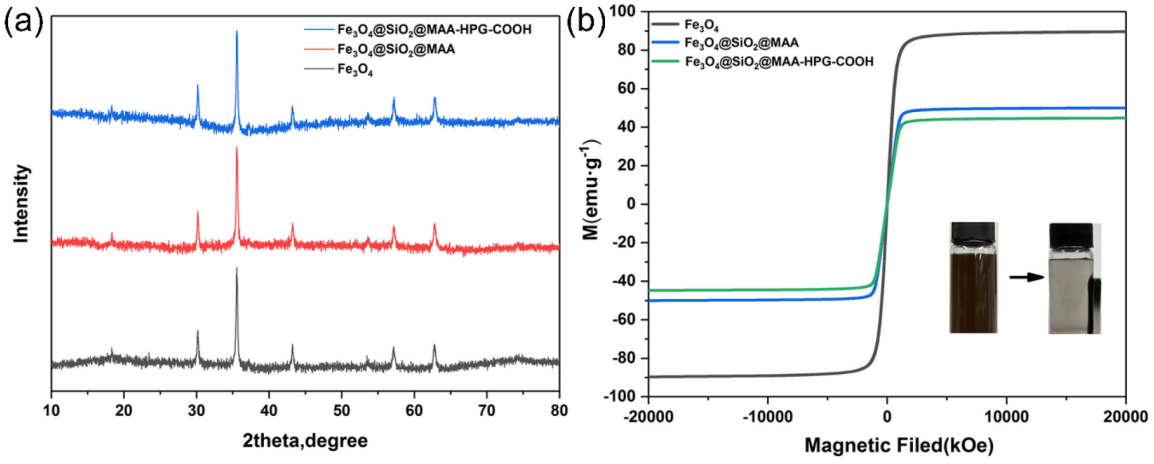

Figure 8. *(a) XRD pattern and (b) VSM curve of Fe_3O_4, Fe_3O_4@SiO_2@MAA, Fe_3O_4@SiO_2@MAA-HPG-COOH. The inset is the corresponding magnetic separation digital photos*

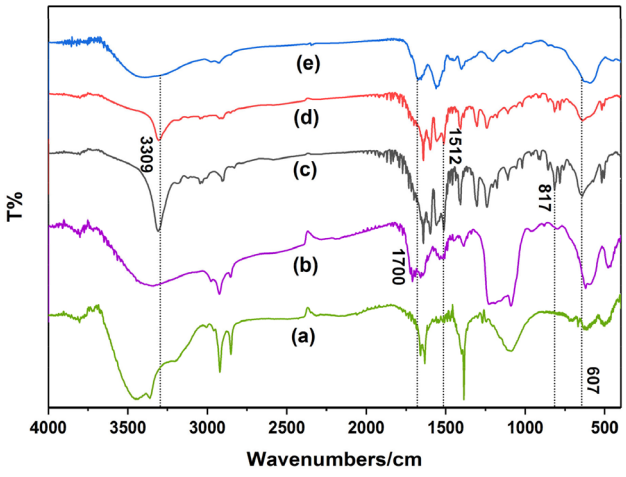

Figure 9. *FTIR spectra of (a) Fe_3O_4, (b) Fe_3O_4@SiO_2@MAA, (c) Fe_3O_4@SiO_2@MAA-MDI, (d) Fe_3O_4@SiO_2@MAA-MDI-HPG and (e) Fe_3O_4@SiO_2@MAA-HPG-COOH*

corresponding to C=O stretching vibration was observed at 1700 cm^{-1} (Figure 9e), indicating that the -OH of HPG was successfully converted to –COOH, which provided active sites for MNPs for further biological coupling.

TG and DLS study

The thermal properties of magnetic nanoparticles were an important factor to evaluate their applicability. Figure 10a showed the thermogravimetric curves of products at different reaction stages in the synthesis route. In Figure 10ai, the weight loss was mainly caused by residual water in Fe_3O_4. Figure 10aii showed that PMAA loses weight in the range of 230-480 °C with a mass loss of about 32%. As can be seen from Figure 10aiii, the compounds formed by MDI, HPG and SA grafted onto magnetic nanoparticles had a slight weight loss of 11.06% at 700-743 °C. The mass of Fe_3O_4 in Fe_3O_4@SiO_2@MAA-HPG-COOH accounted for about 40% and was still undecomposed at 800 °C. The particle size distribution in Figure 10b and Figure 10c was assessed from dynamic light scattering measurement. Figure 10b showed the particle size distribution of the product under the condition of pH=7. It can be clearly seen that the particle size distribution range of the nanoparticles after surface modification was narrow, and the particle size value of Fe_3O_4@SiO_2@MAA-HPG-COOH was 845.04 nm, which was about 200 nm larger than the MNPs photographed by SEM. This may be there were many hydroxyl groups on the hyperbranched structure of HPG on the surface, which formed hydration layer with water molecules and increased particle diameter.

Figure 10c showed the particle size of MNPs in sodium chloride solutions with different concentrations before and after modification, which can reflect its colloidal stability under physiological conditions. The particle size was obtained by placing Fe_3O_4@SiO_2@MAA and Fe_3O_4@SiO_2@MAA-HPG-COOH under different NaCl concentrations of 0-3 mol L^{-1}. When NaCl concentration was 0-3 mol L^{-1}, the particle size of Fe_3O_4@SiO_2@MAA was basically unchanged, while the particle size of Fe_3O_4@SiO_2@MAA was about 3 times of the initial state under the condition of c_{NaCl} = 3 mol L^{-1}. This indicated that the aggregation of Fe_3O_4@SiO_2@MAA -HPG-COOH was smaller and its stability was higher than Fe_3O_4@SiO_2@MAA. In Figure 10d, Fe_3O_4@SiO_2@MAA and Fe_3O_4@SiO_2@MAA-HPG-COOH were dispersed in water at

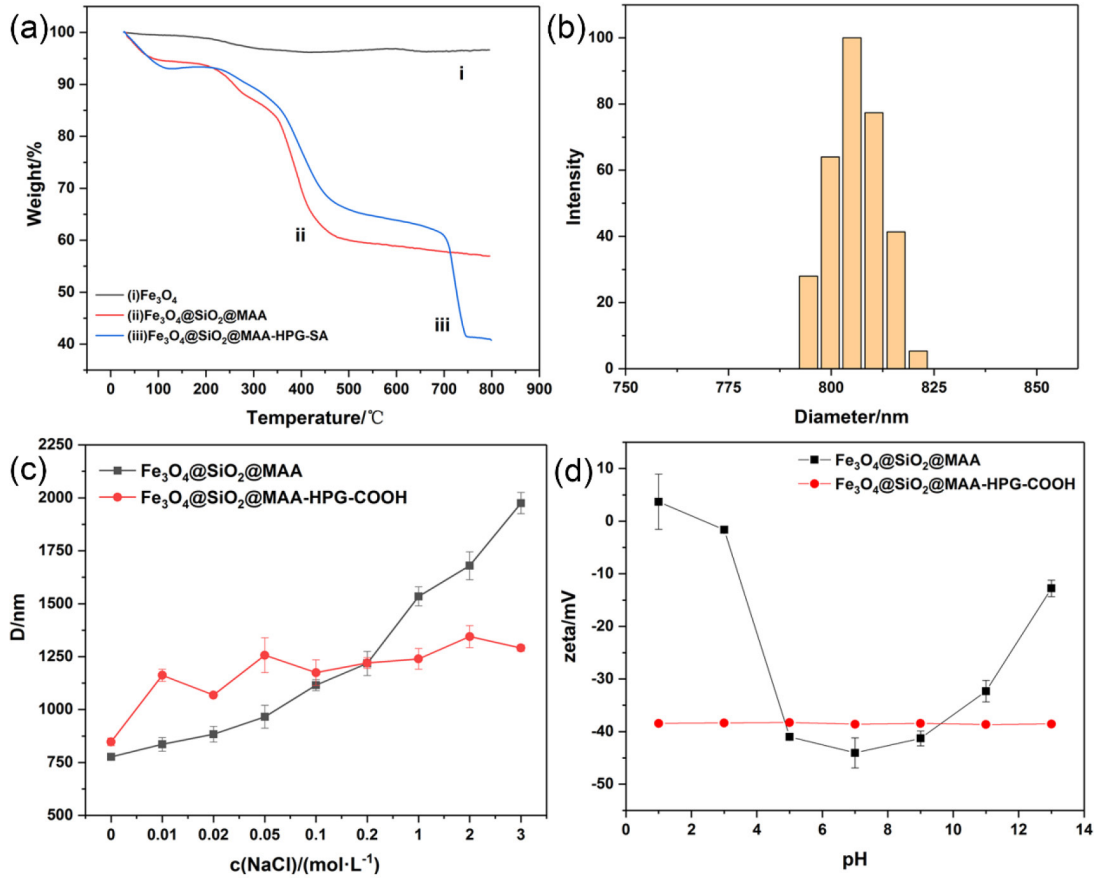

Figure 10. *(a) TG analysis of Fe_3O_4, Fe_3O_4@SiO_2@MAA and Fe_3O_4@SiO_2@MAA-HPG-COOH and (b) size distribution in water about pH=7 and (c) diameter in different sodium chloride concentrations and (d) zeta potential at pH=1-13*

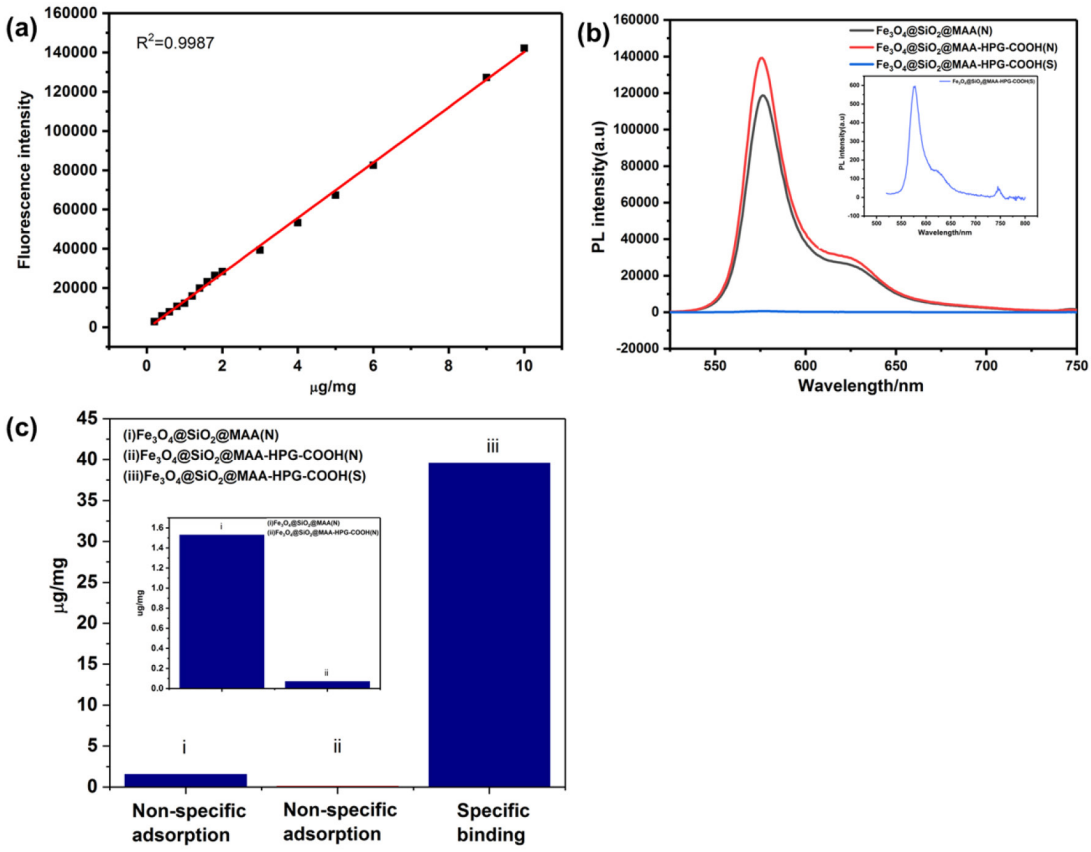

Figure 11. *(a) Standard curve of phycoerythrin solution, (b) the fluorescence spectra of different MNPs supernatant after non-specific adsorption and specific binding of proteins, (c) the amount of non-specific adsorption and specific binding of proteins by different MNPs*

pH=1–13, and Zeta values were recorded to observe the colloid stability. The Zeta potential of Fe_3O_4@SiO_2@MAA-HPG-COOH was less than -30 mV under strong acidic and alkaline conditions, so it can be considered that nanoparticles can exist stably in aqueous solution with pH=1-13.

Surface non-specific adsorption and specific binding

In order to evaluate the non-specific adsorption capacity of proteins, MNPs were added to a certain concentration of phycoerythrin solution for incubation. The protein nonspecific adsorption with different surface properties was studied using phycoerythrin as a model protein. Phycoerythrin had a strong absorption peak at 576 nm at the emission wavelength of 496 nm. The standard curve method was used to calculate the concentration of unknown phycoerythrin solution. The fitting value of the standard curve was R=0.9994 (Figure 11a), indicating that the linear relationship was good within the concentration range of 0-10 μg mL^{-1} phycoerythrin content.

Fe_3O_4@SiO_2@MAA and Fe_3O_4@SiO_2@MAA-HPG-COOH were incubated with phycoerythrin respectively, and the photoluminescence intensity of supernatant was measured with PL (Figure 11b). The results indicated that the non-specific adsorption capacity of the protein Fe_3O_4@SiO_2@MAA was much higher than Fe_3O_4@SiO_2@MAA-HPG-COOH, which indicated that HPG could effectively reduce the non-specific adsorption of the protein, the non-specific adsorption only accounted for 4.58% of the unmodified. Meanwhile, in order to verify that Fe_3O_4@SiO_2@MAA-HPG-COOH had active carboxyl groups on the surface, MNPs were activated by EDC and NHS for specific binding of proteins, and the final specific binding capacity was found to be 39.61 μg mg^{-1} (Figure 11c).[48-50]

Detection of cTnI in the human plasma samples

In order to evaluate the ability of MNPs to reduce non-specific adsorption of proteins and improve specific binding of antigens before and after grafting HPG *in vitro* diagnosis, we prepared Fe_3O_4@SiO_2@MAA and Fe_3O_4@SiO_2@MAA-HPG-COOH into sandwich-type chemiluminescent immunomagnetic respectively.[40-42] and were detected in human plasma samples respectively. The results were shown in the Figure 12. The amount of non-specific adsorption

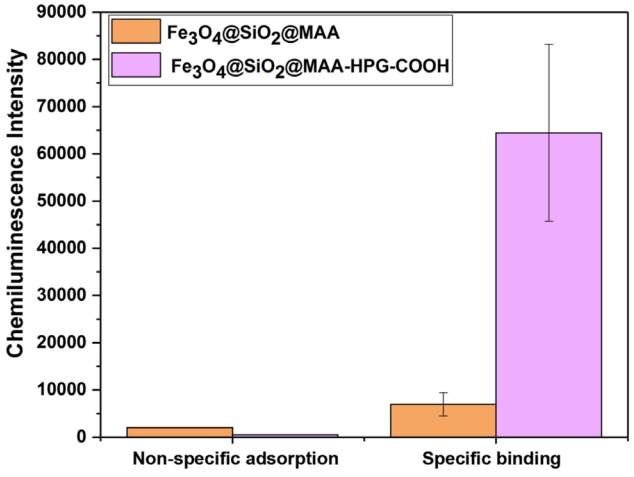

Figure 12. *The chemiluminescence intensity of non-specific adsorption of proteins of Fe_3O_4@SiO_2@MAA, Fe_3O_4@SiO_2@MAA-HPG-COOH and the chemiluminescence intensity of specific binding of antigens of Fe_3O_4@SiO_2@MAA-HPG-COOH*

of the MNPs modified by grafting HPG decreased to 23.64%, and the amount of binding cTnI was 9.27 times higher than the original, indicating that the MNPs modified by grafting HPG had a good prospect *in vitro* diagnostic.

CONCLUSIONS

In this paper, MNPs with a diameter of 600 nm and anti-protein nonspecific adsorption ability were successfully prepared. On the basis of Fe_3O_4@SiO_2@MAA, HPG was grafted to the surface of magnetic nanoparticles through a series of chemical reactions, which can effectively reduce the non-specific adsorption of proteins. Then, the polyhydroxyl group of HPG reacted with maleic anhydride to open the ring of SA, carboxyl groups on the surface of MNPs can provide convenient conjugation sites for biomolecules. The MNPs Fe_3O_4@SiO_2@MAA-HPG-COOH reduced surface nonspecific adsorption, improved colloidal stability and easily bond to biomolecules through surface modification strategies, which can be used for various types of bioseparation and bioanalysis.

ACKNOWLEDGEMENTS

We acknowledge the financial support from Jiangsu Ainaji Neoenergy Science & Technology Co., Ltd. (8507040091), the Fundamental Research Funds for the Central Universities (3207045420), the National Natural Science Foundation of China (81703366).

REFERENCES

1. Ma, W. F.; Li, L. L.; Zhang, Y.; An, Q.; You, L. J.; Li, J. M.; Zhang, Y. T.; Xu, S.; Yu, M.; Guo, J.; Lu, H.-J.; Wang, C.-C.; *J. Mater. Chem.* **2012**, *22*, 23981. [Crossref]
2. Xu, S.; Song, X. J.; Guo, J.; Wang, C. C.; *ACS Appl. Mater. Interfaces* **2012**, *4*, 4764. [Crossref]
3. Zhang, Y. T.; Li, D.; Yu, M.; Ma, W. F.; Guo, J.; Wang, C. C.; *ACS Appl. Mater*. *Interfaces* **2014**, *6*, 8836. [Crossref]
4. Bu, T.; Zako, T.; Zeltner, M.; Sorgjerd, K. M.; Schumacher, C. M.; Hofer, C. J.; Stark, W. J.; Maeda, M.; *J. Mat. Chem. B* **2015**, *3*, 3351. [Crossref]
5. He, K.; Chen, C. Y.; Liang, C. S.; Liu, C.; Yang, B.; Chen, X. M.; Cai, C. Q.; *Sens. Actuators, B* **2016**, *233*, 607. [Crossref]
6. Li, Q.; Wang, B. H.; Wang, J. Q.; Xi, X. J.; Chu, Q.; Dong, G. L.; Wei, Y.; *New J. Chem*. **2017**, *41*, 13673. [Crossref]
7. Wang, B. H.; Shao, Q.; Fang, Y. T.; Wang, J. Q.; Xi, X. J.; Chu, Q.; Dong, G. L.; Wei, Y.; *New J. Chem*. **2017**, *41*, 5651. [Crossref]
8. Cruz-Acuna, M.; Halman, J. R.; Afonin, K. A.; Dobson, J.; Rinaldi, C.; *Nanoscale* **2018**, *10*, 17761. [Crossref]
9. Xu, S.; Yin, B. R.; Guo, J.; Wang, C. C.; *J. Mat. Chem. B* **2013**, *1*, 4079. [Crossref]
10. Kolosnjaj-Tabi, J.; Lartigue, L.; Javed, Y.; Luciani, N.; Pellegrino, T.; Wilhelm, C.; Alloyeau, D.; Gazeau, F.; *Nano Today* **2016**, *11*, 280. [Crossref]
11. Nappini, S.; Fogli, S.; Castroflorio, B.; Bonini, M.; Bombelli, F. B.; Baglioni, P.; *J. Mat. Chem. B*. **2016**, *4*, 716. [Crossref]
12. Huang, H. L.; Wang, X. H.; Ge, H.; Xu, M.; *ACS Sustainable Chem. Eng*. **2016**, *4*, 3334. [Crossref]
13. Lian, L. L.; Lv, J. Y.; Lou, D. W.; *ACS Sustainable Chem. Eng.* **2017**, *5*, 10298. [Crossref]
14. Han, J.; Wang, L.; Wang, Y.; Cai, Y. F.; Mao, Y. L.; Ni, L.; Xie, X. Q.; *Food Bioprod. Process*. **2019**, *114*, 253. [Crossref]
15. Han, J.; Wang, L.; Wang, L.; Li, C. M.; Mao, Y. L.; Wang, Y.; *Food Chem*. **2019**, *283*, 1. [Crossref]
16. Xu, S.; Weng, Z. H.; Tan, J.; Guo, J.; Wang, C. C.; *Polym. Chem*. **2015**, *6*, 2892. [Crossref]
17. Luo, J. X.; Zhang, X. C.; Zhang, C. Y.; Wang, T.; Chen, X.; Chen, H. Y.; King, S.; Wang, C. C.; *Chin. Chem. Lett*. **2019**, *30*, 2043. [Crossref]
18. Chamchoy, K.; Inprasit, T.; Vanichvattanadecha, C.; Thiangtrong, A.; Anukunwithaya, P.; Pisitsak, P.; *J. Polym. Environ*. **2020**, *29*, 484. [Crossref]
19. Liu, H. X.; Xie, X. J.; *Environ. Sci. Pollut. Res.* **2021**, *28*, 42750. [Crossref]
20. Men, J. Y.; Shi, H. X.; Dong, C. Y.; Yang, Y. Y.; Han, Y. R.; Wang, R. X.; Zhang, Y. Q.; Zhao, T.; Li, J.; *Int. J. Biol. Macromol*. **2021**, *181*, 810. [Crossref]
21. Ugelstad, J.; Stenstad ,P.; Kilaas, L.; Prestvik, W.-S.; Herje, R.; Berge, A.; Hornes, E.; *Blood Purif*. **1996**, *11*, 349. [Crossref]
22. Lin, R.; Li, Y.; MacDonald, T.; Wu, H.; Provenzale, J.; Peng, X.; Huang, J.; Wang, L.; Wang, A. Y.; Yang, J.; Mao, H.; *Colloids Surf., B* **2017**, *150*, 261. [Crossref]
23. He, Q. J.; Zhang, J. M.; Shi, J. L.; Zhu, Z. Y.; Zhang, L. X.; Bu, W. B.; Guo, L. M.; Chen, Y.; *Biomaterials* **2010**, *31*, 1085. [Crossref]
24. Hlidkova, H.; Horak, D.; Proks, V.; Kucerova, Z.; Pekarek, M.; Kucka, J.; *Macromol. Biosci.* **2013**, *13*, 503. [Crossref]
25. Liu, Y.; Gao, D.; Zhang, X.; Liu, Z.; Dai, K.; Ji, B.; Wang, Q.; Luo, L.; *Mater. Sci. Eng., C* **2016**, *64*, 124. [Crossref]
26. Aslund, A. K. O.; Sulheim, E.; Snipstad, S.; von Haartman, E.; Baghirov, H.; Starr, N.; Lovmo, M. K.; Lelu, S.; Scurr, D.; Davies, C. de L.; Schmid, R.; Mørch, Ý.; *Mol. Pharm*. **2017**, *14*, 2560. [Crossref]
27. Dong, X. J.; Zhang, Z. L.; Wu, L. L.; Ma, X. Y.; Xu, C. M.; Pang, D. W.; *ACS Omega* **2019**, *4*, 7391. [Crossref]
28. Shutava, T. G.; Livanovich, K. S.; Sharamet, A. A.; *Colloids Surf., B* **2019**, *173*, 412. [Crossref]
29. Xiao, W. C.; Lin, J.; Li, M. L.; Ma, Y. J.; Chen, Y. X.; Zhang, C. F.; Li, D.; Gu, H. C.; *Contrast Media Mol. Imaging*. **2012**, *7*, 320. [Crossref]
30. Lu, C. C.; Zhao, D. P.; Wang, S.; Wang, Y. M.; Wang, Y. N.; Gao, H.; Ma, J. B.; Wu, G. L.; *RSC Adv*. **2014**, *4*, 20665. [Crossref]
31. Hu, F. L.; Chen, K. M.; Xu, H.; Gu, H. C.; *Colloids Surf., B* **2015**, *126*, 251. [Crossref]
32. Zhang, L. P.; Wu, L. Y.; Shi, G.; Sang, X. X.; Ni, C. H.; *J. Biomater. Sci., Polym. Ed*. **2018**, *29*, 646. [Crossref]
33. Lee, G.; Song, J.; Han, H.; Kwon, D.; Park, J.; Jeon, S.; Jeong, S.; Kim, S.; *Bioconjugate Chem*. **2021**, *32*, 1052. [Crossref]
34. He, Q. J.; Zhang, J. M.; Shi, J. L.; Zhu, Z. Y.; Zhang, L. X.; Bu, W. B.; Guo, L. M.; Chen, Y.; *Biomaterials* **2010**, *31*, 1085. [Crossref]
35. Wang, L.; Su, D.; Zeng, L. T.; Liu, N.; Jiang, L.; Feng, X. Q.; Neoh, K. G.; Kang, E. T.; *Dalton Trans*. **2013**, *42*, 13642. [Crossref]
36. He, Y.; Cheng, Z.; Qin, Y.; Xu, B.; Ning, L.; Zhou, L.; *Mater. Lett*. **2015**, *151*, 100. [Crossref]
37. Li, M.; Neoh, K. G.; Wang, R.; Zong, B. Y.; Tan, J. Y.; Kang, E. T.; *Eur. J. Pharm. Sci.* **2013**, *48*, 111. [Crossref]
38. Wang, S.; Zhou, Y.; Yang, S.; Ding, B.; *Colloids Surf., B* **2008**, *67*, 122. [Crossref]
39. Irvine, D. J.; Mayes, A. M.; Griffith-Cima, L.; *Macromolecules* **1996**, *29*, 6037. [Crossref]
40. Zhao, H.; Lin, Q. F.; Huang, L.; Zhai, Y. F.; Liu, Y.; Deng, Y.; Su, E. B.; He, N. Y.; *Nanoscale* **2021**, *13*, 3275. [Crossref]
41. Fu, H.-J.; Yuan, L.-P.; Shen, Y.-D.; Liu, Y.-X.; Liu, B.; Zhang, S.-W.; Xie, Z.-X.; Lei, H.-T.; Sun, Y.-M.; Xu, Z.-L.; *Anal. Chim. Acta* **2018**, *1035*, 129. [Crossref]
42. Wang, J. Y.; Wang, X. Q.; Ren, L.; Wang, Q.; Li, L.; Liu, W. M.; Wan, Z. F.; Yang, L. Y.; Sun, P.; Ren, L.; Li, M.; Wu, H.; Wang, J.; Zhang, L.; *Anal. Chem.* **2009**, *81*, 6210. [Crossref]
43. Liu, B.; Zhang, W.; Yang, F. K.; Feng, H. L.; Yang, X. L.; *J. Phys. Chem. C* **2011**, *115*, 15875. [Crossref]

44. Jurikova, A.; Csach, K.; Miskuf, J.; Koneracka, M.; Zavisova, V.; Kubovcikova, M.; Kopcansky, P.; Muckova, M.; *IEEE Trans. Magn.* **2013**, *49*, 236. [Crossref]
45. Kucerova, J.; Svobodova, Z.; Knotek, P.; Palarcik, J.; Vlcek, M.; Kincl, M.; Horak, D.; Autebert, J.; Viovy, J. L.; Bilkova, Z.; *Mater. Sci. Eng., C* **2014**, *40*, 308. [Crossref]
46. Aragón, F. H.; Coaquira, J. A. H.; Villegas-Lelovsky, L.; da Silva, S. W.; Cesar, D. F.; Nagamine, L. C. C. M.; Cohen, R.; Menéndez-Proupin, E.; Morais, P. C.; *J. Phys.: Condens. Matter* **2015**, *27*, 095301. [Crossref]
47. Piazza, D. B.; Viali, W. R.; dos Santos, C. C.; Nunes, E. S.; Marques, R. F. C.; Morais, P. C.; da Silva, S. W.; Coaquira, J. A. H.; Jafelicci, M.; *Mater. Res. Express* **2020**, *7*, 015078. [Crossref]
48. Macaroff, P. P.; Oliveira, D. M.; Lacava, Z. G. M.; Azevedo, R. B.; Lima, E. C. D.; Morais, P. C.; Tedesco, A. C.; *IEEE Trans. Magn.* **2004**, *40*, 3027. [Crossref]
49. Macaroff, P. P.; Simioni, A. R.; Lacava, Z. G. M.; Lima, E. C. D.; Morais, P. C.; Tedesco, A. C.; *J. Appl. Phys.* **2006**, *99*, 08S102. [Crossref]
50. Primo, F. L.; Macaroff, P. P.; Lacava, Z. G. M.; Azevedo, R. B.; Morais, P. C.; Tedesco, A. C.; *J. Magn. Magn. Mater.* **2007**, *310*, 2838. [Crossref]